Clay Minerals (2024), 1–13
doi:10.1180/clm.2024.6

CAMBRIDGE UNIVERSITY PRESS

Article

Moroccan heated clay-based geopolymer reinforced with date palm cellulose: microstructure characterization and mechanical/physical properties

Abdellah Mourak and Mohamed Hajjaji

Laboratoire des Sciences des Matériaux et Optimisation des Procédés, Faculté des Sciences Semlalia, Université Cadi Ayyad, Marrakech, Morocco

Abstract

The objective of this research was to study the cellulose addition effect on the geopolymerization of heated clay. The clay, composed of illite, plagioclase and kaolinite, was heated at 700°C for 2 h and mixed with cellulose (up to 10 mass%). The mixtures were NaOH-activated, and shaped samples were aged at 83°C for 30 days. The cured samples were investigated by using X-ray diffraction, Fourier-transform infrared spectroscopy and scanning electron microscopy. The influence of the cellulose addition on the mechanical/physical properties was also evaluated. The results showed that zeolite ZK-14, hydrosodalite, sodium carbonate and a geopolymer composed of poly(sialate) units were formed in all cured samples. The relative amounts of zeolite and metakaolin evolved antagonistically, whereas that of illite slightly decreased with increasing cellulose content. Metakaolin and illite were involved in the geopolymerization process. Cellulose addition led to the improvement of the flexural strength of the samples and to porosity reduction. By contrast, water absorption was increased. The positive effect of cellulose on sample performance is explained on the basis of hydrogen bonding between the functional moieties of cellulose and the active sites of sample constituents, namely zeolites, metakaolin, illite and the geopolymer. As a filler, zeolite probably contributed to sample strengthening, and the detrimental impact of Na-carbonate was insignificant. Based on the results obtained, the composites could be used as binders for brick manufacturing or as lightweight mortars.

Keywords: Cellulose; geopolymer; heated clay; microstructure; sample performances

(Received 5 December 2023; revised 10 February 2024; accepted 17 February 2024; Accepted Manuscript online: 26 February 2024; Associate Editor: Chunhui Zhou)

Recently, major concern has been expressed regarding ordinary Portland cement (OPC) manufacturing because of the huge amounts of carbon dioxide it releases (Zhang *et al.*, 2023), the energy required and the scarcity of the geomaterials needed. Therefore, research has been undertaken worldwide to find eco-friendly cementitious materials with good physical and mechanical properties (Mohamad *et al.*, 2022; da Silva Rego *et al.*, 2023; Shi *et al.*, 2023). Geopolymers, which are low-temperature synthesized aluminosilicates, have been considered as potential alternatives to OPC (Ranjbar *et al.*, 2020; Giacobello *et al.*, 2022; Tanu *et al.*, 2022; Ayub & Khan, 2023; Jwaida *et al.*, 2023). Fly ash, calcined clays, volcanic ash and blast furnace slag are amongst the used aluminosilicate sources for geopolymer synthesis. For the latter purpose, these materials are dissolved using moderate to strong alkaline solutions (4–12 M). NaOH is by far the most used alkali-hydroxide activator. Mixtures of NaOH and Na_2SiO_3 are also used. In the latter condition, OH^- ions (NaOH-derivative species) are involved in the dissolution of the aluminosilicate, whilst sodium silica plays the role of a binder (Mijarsh *et al.*, 2015). Na^+ ions contribute to the charge balance as well as to zeolite formation. The excess of Na^+ ions induces the formation of carbonate by reaction with atmospheric carbon dioxide. Such a phenomenon occurs particularly in the case of the NaOH-activated metakaolin system (Valentini, 2018).

Considering metakaolin, for instance, which is considered to be a high-grade source material for geopolymer synthesis, alkali activation resulted in the formation of $Al(OH)_4^-$, $H_3SiO_4^-$ and $H_2SiO_4^{2-}$ species (Valentini, 2018; Weng & Sagoe-Crentsil, 2007) together with a sodium aluminosilicate hydrate (Na_2O–Al_2O_3–SiO_2–H_2O gel; Valentini, 2018). According to Weng & Sagoe-Crentsil (2007), the association of $Al(OH)_4^-$ and $H_2SiO_4^{2-}$ results in the formation of small oligomers (dimers and trimers). However, the condensation between $Al(OH)_4^-$ and $H_3SiO_4^-$ leads to the formation of polymers and larger oligomers. The latter products consist of linked silica ($[SiO_4]^{4-}$) and alumina ($[AlO_4]^{4-}$) tetrahedra. The three-dimensional structure obtained is called a geopolymer (Van Deventer *et al.*, 2007; Sotelo-Piña *et al.*, 2019; Almutairi *et al.*, 2021).

Cellulose is one of the main constituents of plants. It exists as fibres and has a polymeric structure. Cellulose chains are composed of β-D-glucose units, and their organization into sheets is achieved due to its methylol ($-CH_2OH$) and the hydroxyl moieties (Bashline *et al.*, 2014; Etale *et al.*, 2023). Cellulose fibres have high strength/density ratios (Chen *et al.*, 2021; Emenike *et al.*, 2023). Therefore, they have been proven to be suitable for reinforcing some matrix materials (Ferreira *et al.*, 2021; Mourak *et al.*, 2021; Lazorenko *et al.*, 2022; Zheng *et al.*, 2023). Cellulose's reinforcing capability is mainly influenced by its

Corresponding author: Abdellah Mourak; Email: abdellahmourak340@gmail.com
Cite this article: Mourak A, Hajjaji M. Moroccan heated clay-based geopolymer reinforced with date palm cellulose: microstructure characterization and mechanical/physical properties. *Clay Minerals*. https://doi.org/10.1180/clm.2024.6

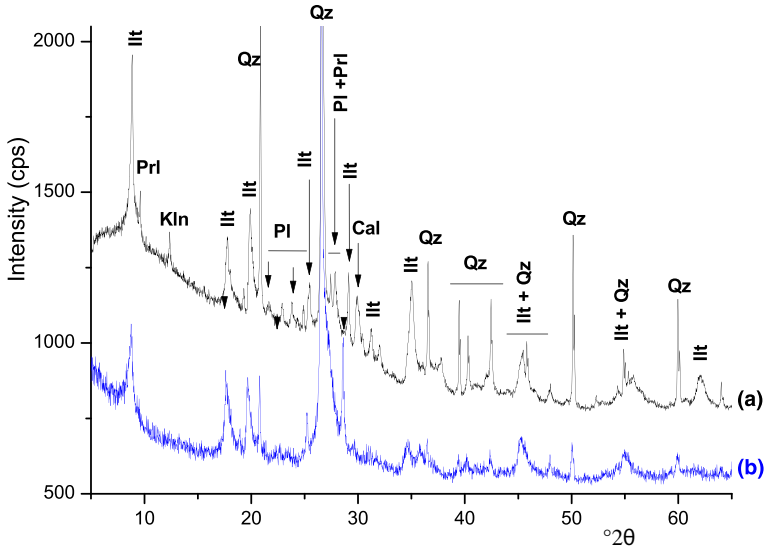

Figure 1. X-ray diffraction traces of the (a) raw and (b) heated clays. Cal = calcite (PDF#83-1762); cps = counts per second; Ilt = illite (PDF# 43-0685); Kln = kaolinite (PDF# 83-0971); Pl = plagioclase (PDF# 41-1486); Prl = pyrophyllite (PDF# 96-0277); Qz = quartz (PDF# 05-0490).

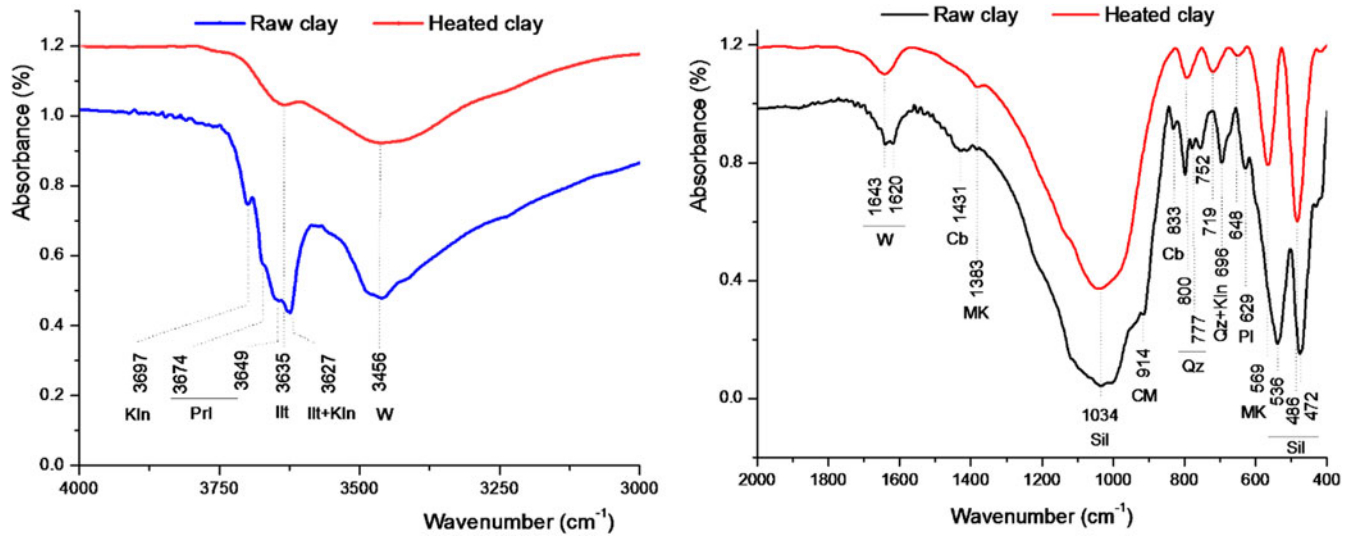

Figure 2. Fourier-transform infrared spectra of the raw and heated clays. cb = carbonates; CM = clay minerals; Ilt = illite; Kln = kaolinite; MK = metakaolin; Pl = plagioclase; Prl = pyrophyllite; Qz = quartz; Sil = silicates; W = water.

fibre dimensions, surface properties and moisture retention (Farhan *et al.*, 2021; Santana *et al.*, 2021). According to some studies, the addition of cellulose to cementing materials should be limited (0.2–2.0% v/v; Jamshaid *et al.*, 2022; Raghunath *et al.*, 2023; de Souza *et al.*, 2023; dos Reis *et al.*, 2023). The addition of large amounts of cellulose resulted in increased water adsorption, and consequently the mechanical strength of the cellulose-containing cementing materials decreased (Singh & Gupta, 2020; Jaberizadeh *et al.*, 2023).

The reinforcing effect of the cellulose fibres can be improved by alkali activation using NaOH solutions (18–32 mass%) at 25–40°C. Due to this chemical treatment, fibrils with large surface areas and high aspect ratios form, and consequently adhesion between the reinforcing material and the matrix is enhanced (Aravindh *et al.*, 2022; Asyraf *et al.*, 2022).

Considering the above literature data, this work of research, which aimed to investigate the microstructure and determine the mechanical/physical properties of heated clay-based geopolymer samples, has fundamental and application interests. Regarding the latter interest, this work is a contribution to the development of eco-friendly clay-based building materials demonstrating acceptable performance. The raw materials (clay and palm date rachis) used are found globally, and the product preparation process does not require sophisticated plants or as much energy as for OPC manufacturing (Semugaza *et al.*, 2023). Fundamentally, this study is a contribution to the understanding of the chemical interactions that could occur between cellulose's functional moieties and the active sites of geopolymers and associated aluminosilicates (zeolite, illite and metakaolin).

Materials and methods

Clay material and cellulose

The raw clay material was from Kharrou Mountain (Rehamna, Morocco). It was essentially composed of mica/illite, pyrophyllite, kaolinite, plagioclase and calcite (Figs 1 & 2). As an aluminosilicate-rich material (Table 1), the clay seemed to be

https://doi.org/10.1180/clm.2024.6 Published online by Cambridge University Press

Table 1. Chemical composition (mass%) of the used clay, the relative amounts of the date palm rachis constituents and the physical characteristics of the extracted cellulose.

Clay								
SiO_2	Al_2O_3	TiO_2	Fe_2O_3	MnO	MgO	K_2O	CaO	Na_2O
56.75	33.74	1.80	1.24	0.01	0.58	2.50	0.27	1.76
Date palm rachis constituents								
Lignin		Hemicellulose		Cellulose			Balance	
20		30.5		47.5			2	
Physical characteristics of the extracted cellulose								
Crystallinity index (%)		Average molecular weight (g mol^{-1})		Polymerization degree				
67		144 622		892				

suitable as a precursor for geopolymer preparation. Therefore, the clay was the object of mechanical and heating treatments, as detailed below. As a result of heating, the kaolinite disappeared and metakaolin was formed (Figs 1 & 2), whereas the illite resisted heating as its structure breaks down at >900°C (Gualtieri & Ferrari, 2006). As can be deduced from the thermograms given in Fig. 3, kaolinite underwent dehydroxylation at ~523°C. In this respect, it should be noted that the differential thermal analysis (DTA) curve showed endothermic phenomena at ~88°C and 272°C, which were assigned to the losses of hygroscopic and strongly retained waters. The weak endothermic peak at 812°C was associated with calcite decomposition.

The cellulose used as reinforcement was extracted from date palm (*Phoenix dactylifera*) rachis following the steps shown in Fig. 4. More details regarding the cellulose extraction are given below. The physical characteristics of the isolated cellulose, which manifested as shown in Fig. 5, are provided in Table 1.

Sample preparation

For geopolymer synthesis, dried portions of the clay heated at 700°C for 2 h and cellulose (up to 10 mass%) were introduced in a glass container and mixed for 15 min. The blend was transferred to a plastic bag and mixed with NaOH solution (6 M). The optimal (NaOH solution volume)/(blend weight) ratio was of 12.5 mL 100 g^{-1}. The paste was kneaded for 15 min (to obtain a plastic paste), and the shaping operation was manually accomplished in ~20 min. The shaped samples (3.8 × 9.2 × 40 mm) were placed in a Memmert oven and aged at 83°C for 30 days. The oven used was functioning in the open air. Regarding the adopted curing conditions, it can be noted that, according to Mo *et al.* (2014), increasing the curing temperature (up to 100°C) accelerates the dissolution, polymerization and reprecipitation processes of the geopolymerization reaction. Through this, the physical/mechanical properties of the product are enhanced. The effect of curing time on geopolymerization is still under debate (Heah *et al.*, 2011; Van Jaarsveld *et al.*, 2022). The NaOH activation solution was prepared by dissolution of NaOH pellets (Sigma-Adrich product, purity: >97.0%) in distilled water.

Experimental procedures and instruments

The raw clay was crushed and ground using an agate mortar then passed through a 100 µm sieve. The sieved fraction was heated in a Nabertherm furnace. The heating conditions were as follows: heating rate: 7°C min^{-1}; maximum temperature: 700°C; soaking time: 2 h; atmosphere: air.

For cellulose extraction, the pigments and lipids associated with cellulose were removed using an azeotropic mixture of ethanol and toluene. The solvent extraction was performed using a conventional Soxhlet extractor. The hemicelluloses and lignin were eliminated using a solution of sodium hydroxide (2 mass%) and *via* heating at 80°C for 2 h. Fibre bleaching was achieved with a solution of sodium chlorite (1.7% w/v) at 70°C (Mourak *et al.*, 2021).

The polymerization degree (PD) of the extracted cellulose was calculated using Equation 1:

$$PD = (AMW)/M_C \quad (1)$$

where AMW is the average molecular weight (144 622 g mol^{-1}) and M_C is the molecular weight of cellulose (162.14 g mol^{-1}). AMW

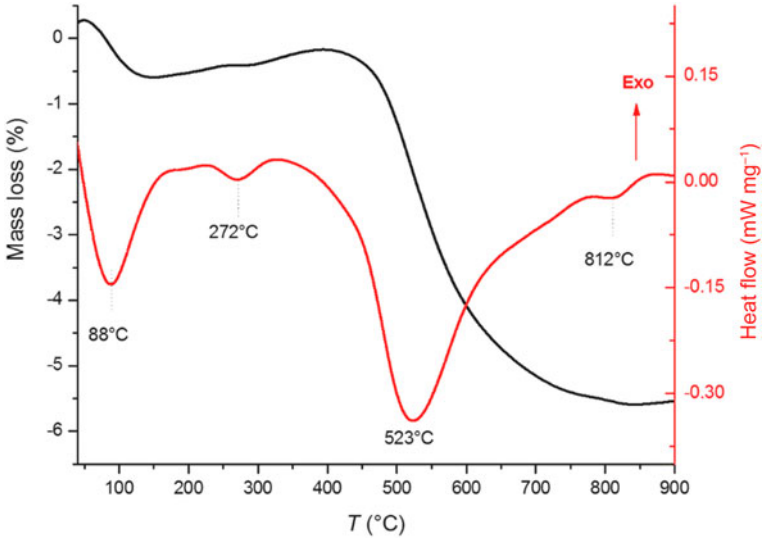

Figure 3. Thermal curves (TG, DTA) of the raw clay.

https://doi.org/10.1180/clm.2024.6 Published online by Cambridge University Press

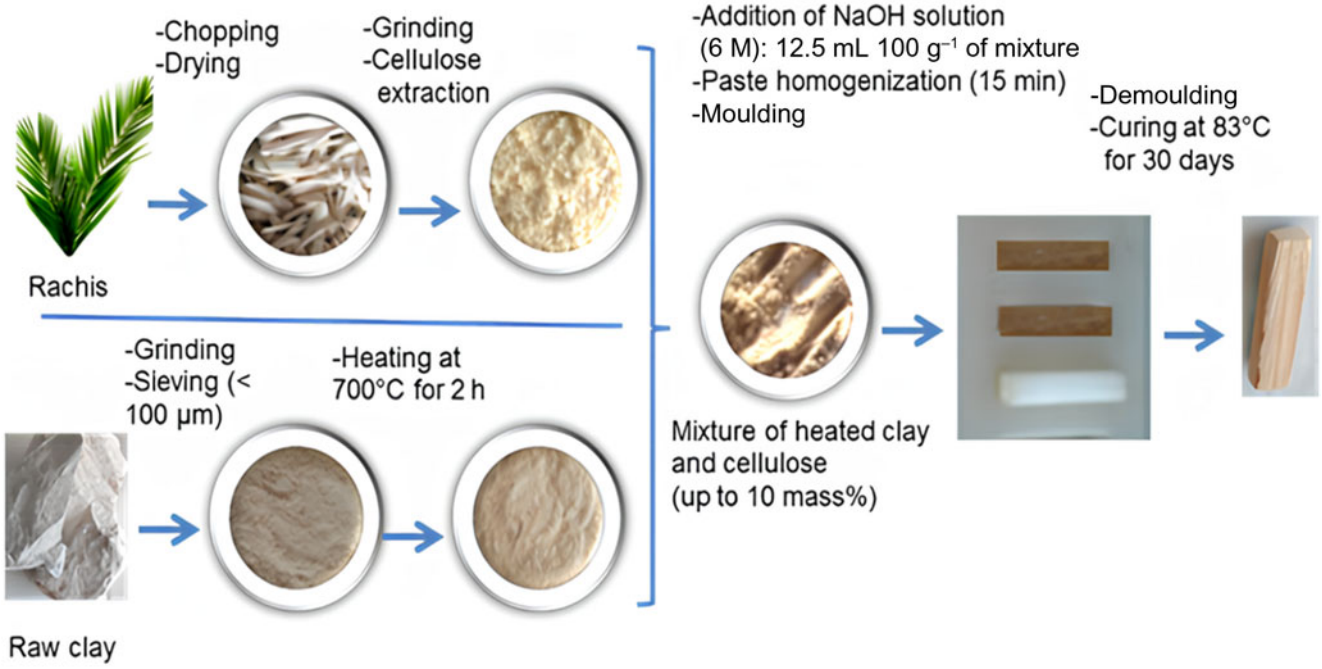

Figure 4. Main steps followed for date palm rachis and raw clay treatments and experimental operations for heated clay–cellulose sample preparation.

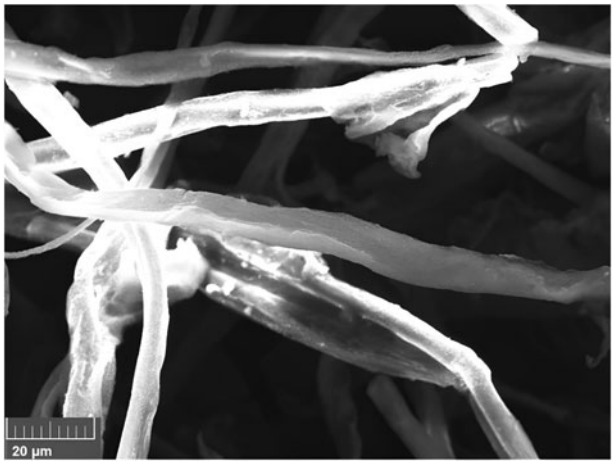

Figure 5. Scanning electron microscopy images showing the cellulose fibre morphology.

was measured following a procedure detailed elsewhere (Evans *et al.*, 1989; Malešič *et al.*, 2021).

As compared with the literature data (Hallac & Ragauskas, 2011), the PD obtained was of low to moderate value. It is believed that cellulose extracted with such a PD value can be used without significant agglomeration tendency.

The crystallinity index (CI) was determined by using data obtained from the X-ray diffraction (XRD) trace of cellulose and Equation 2 (Segal, 1957):

$$\mathrm{CI} = \frac{I_{200} - I_{\mathrm{am}}}{I_{200}} \tag{2}$$

where I_{200} is the maximum intensity of the (200) lattice diffraction and I_{am} is the intensity diffraction at 18°2θ.

The XRD analysis was performed on powder samples using a Rigaku Smart Lab diffractometer operating with a copper anode ($\lambda_{K\alpha} = 1.5418$ Å). The XRD traces were recorded under the following conditions: generator voltage: 40 kV; tube current: 30 mA; scan step size: 0.05°; time step: 2s.

For the Fourier-transform infrared (FTIR) spectroscopy investigation, thin discs (study sample: 1 mg; KBr: 99 mg) were shaped and analysed using a Perkin Elmer 1725-x spectrophotometer functioning in the range of 4000–400 cm^{-1}. *PeakFit* v4.12 software was used for infrared band deconvolution. The best curve fit was evaluated on the basis of the following statistical parameters: correlation coefficient (r^2), standard error (SE) and the Fisher ratio (F-statistic). The relative quantities of metakaolin, zeolite and illite were determined on the basis the areas of their FTIR bands. The areas were evaluated using *PeakFit* software.

For thermal analysis, a SetaramSetsys 24 apparatus was used. The operating conditions were as follows: atmosphere: air; heating rate: 10°C min^{-1}; reference material and crucible: alumina; sample mass: 78 mg.

The microstructure of carbon-coated cured samples was investigated using a TESCAN VEGA3 electron microscope, which was equipped with 20 mm^2 X-Max diffusion silicon detector.

The flexural strength (σ_{FS}) of the samples was evaluated using an EX 150 DeltaLab apparatus (loading rate: 12×10^{-3} kN s^{-1}) and Equation 3:

$$\sigma_{\mathrm{FS}} = \frac{3FL}{2bh^2} \tag{3}$$

where F is the load at failure, L is the distance between the two supports (2.8 cm) of the apparatus and b and h are the width and the thickness of the tested samples, respectively. The measurements were carried out in triplicate, and the standard deviations were in the range of 0.1–0.7 MPa.

https://doi.org/10.1180/clm.2024.6 Published online by Cambridge University Press

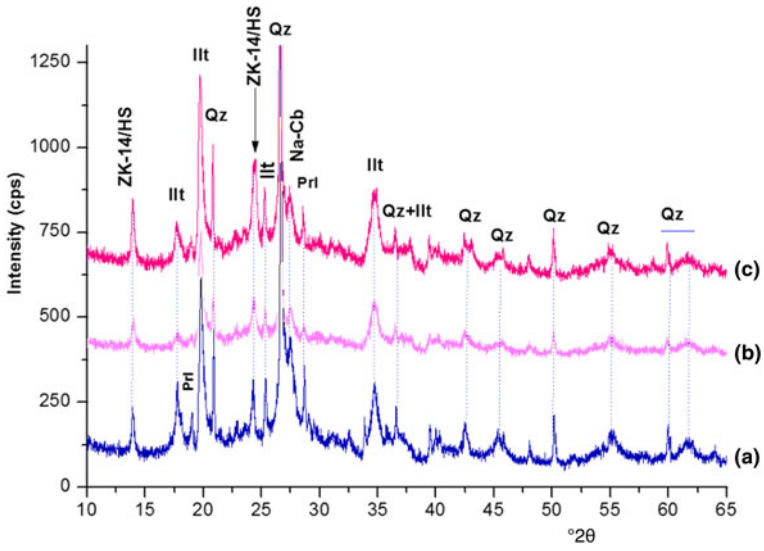

Figure 6. XRD traces of the cured samples: (a) cured cellulose-free samples; (b): cured heated clay–5 mass% cellulose; (c): cured heated clay–10 mass% cellulose. Cb = carbonate (PDF# 86-0298); HS = hydrosodalite (PDF# 76-1639); Ilt = illite (PDF# 43-0685); Prl = pyrophyllite (PDF# 96-0277); Qz = quartz (PDF# 05-0490); ZK-14 = zeolite ZK-14 (PDF# 84-0698).

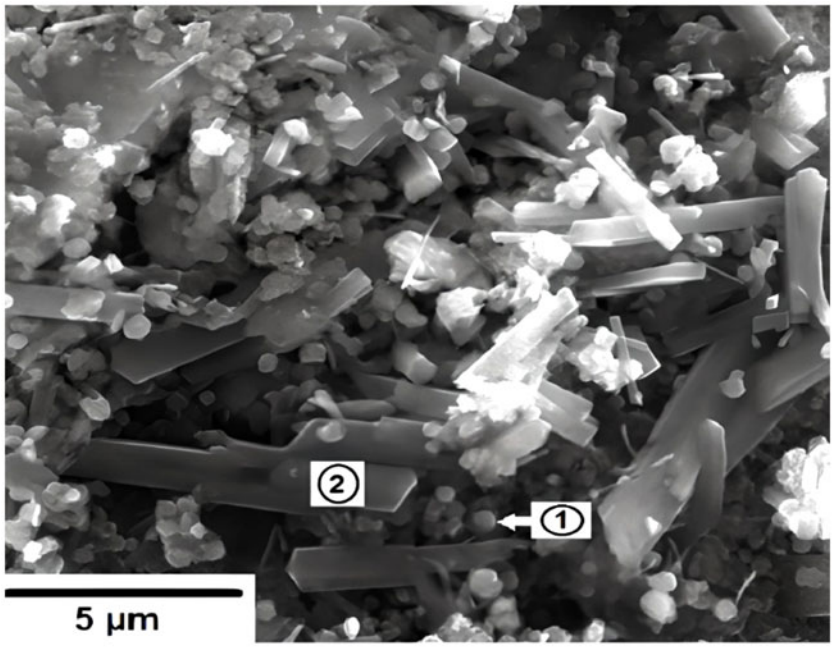

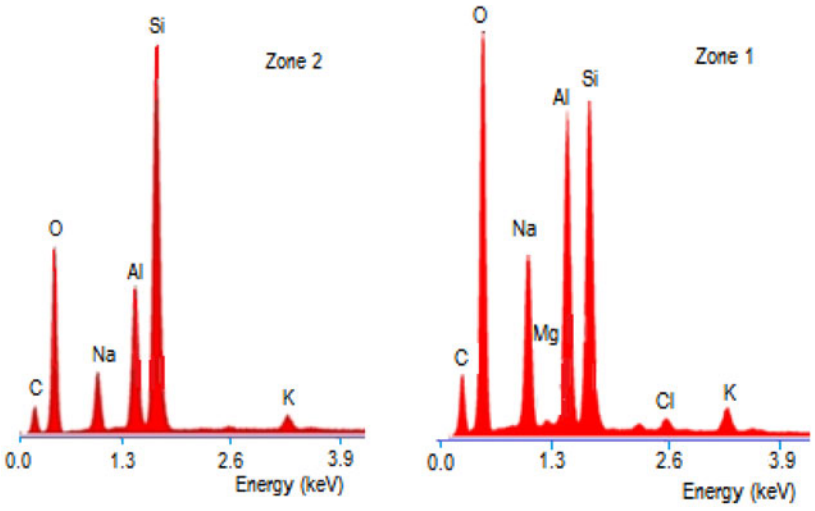

Figure 7. SEM image showing the typical microstructure of the cured sample (10 mass% cellulose) and energy-dispersive spectroscopy spectra associated with hydrosodalite (zone 1) and zeolite ZK-14 (zone 2).

https://doi.org/10.1180/clm.2024.6 Published online by Cambridge University Press

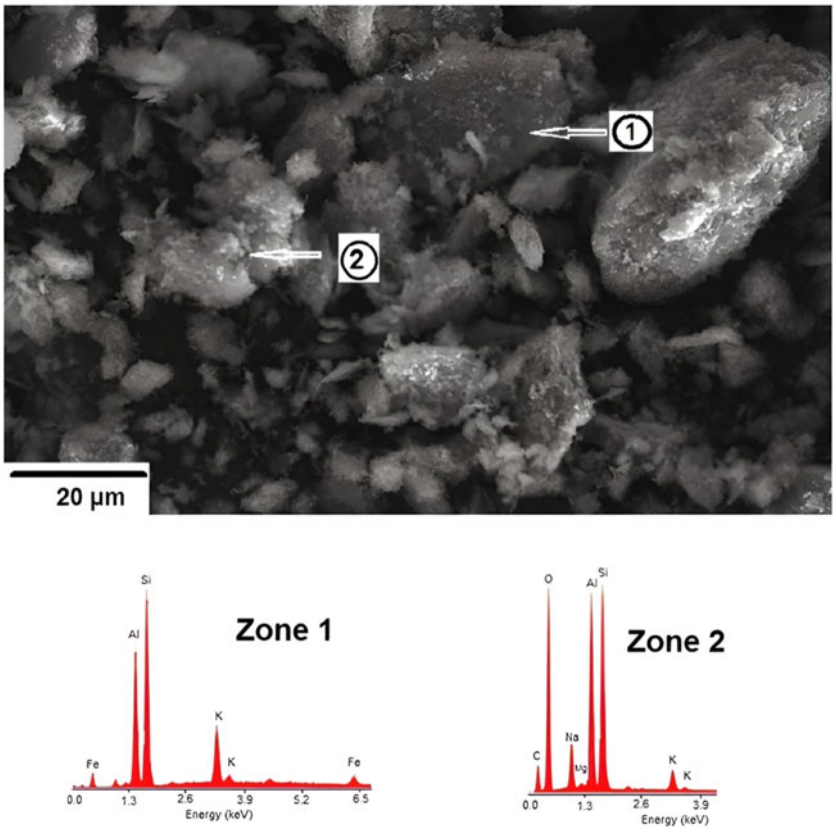

Figure 8. SEM image showing unreacted illite particles (zone 1) and the geopolymer-rich domain (zone 2) and their energy-dispersive spectroscopy spectra.

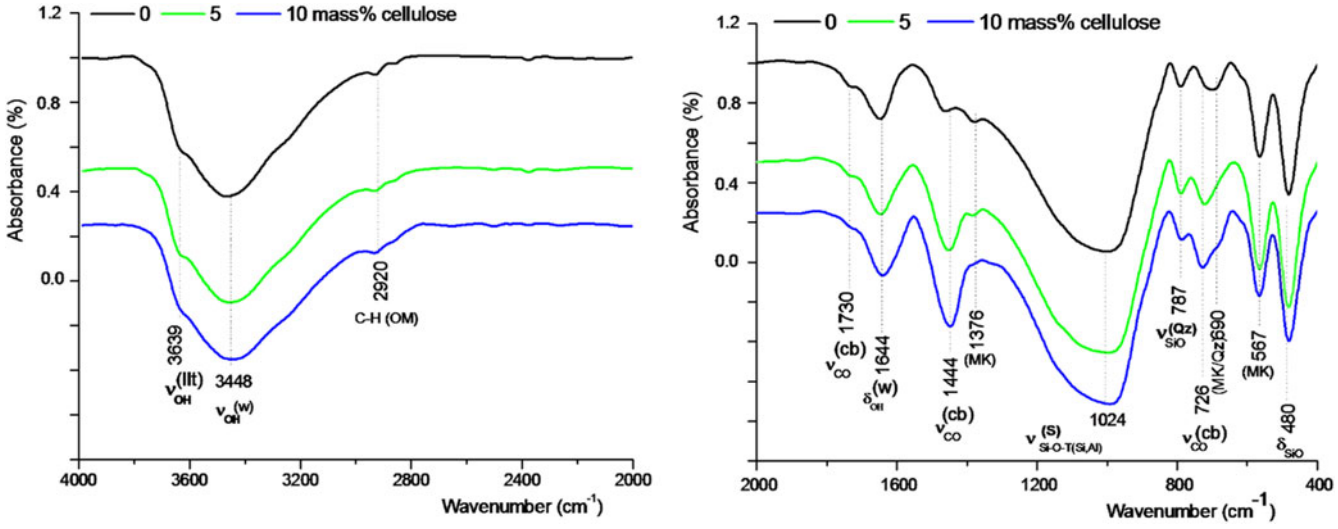

Figure 9. FTIR spectra of the cured cellulose-free sample (0% mass cellulose) and cured cellulose-containing samples (5 and 10 mass% cellulose). For clarification, the O–H stretching vibration zone and the fingerprint region are separated. cb = carbonates; Ilt = illites; MK = metakaolin; OM = organic matter; Qz = quartz; S = silicates; W = water.

The total porosity (P_T) of the samples was calculated according to Equation 4:

$$P_T = 100\left(1 - \frac{\rho_a}{\rho_t}\right) \quad (4)$$

where ρ_a and ρ_t are the apparent and true densities, which were measured using the pycnometry method.

The maximum amount of water retained by the samples (saturation time: 5 min) was determined by weighing the samples before and after contact with water. A water-submerged sponge was used as a source of water.

https://doi.org/10.1180/clm.2024.6 Published online by Cambridge University Press

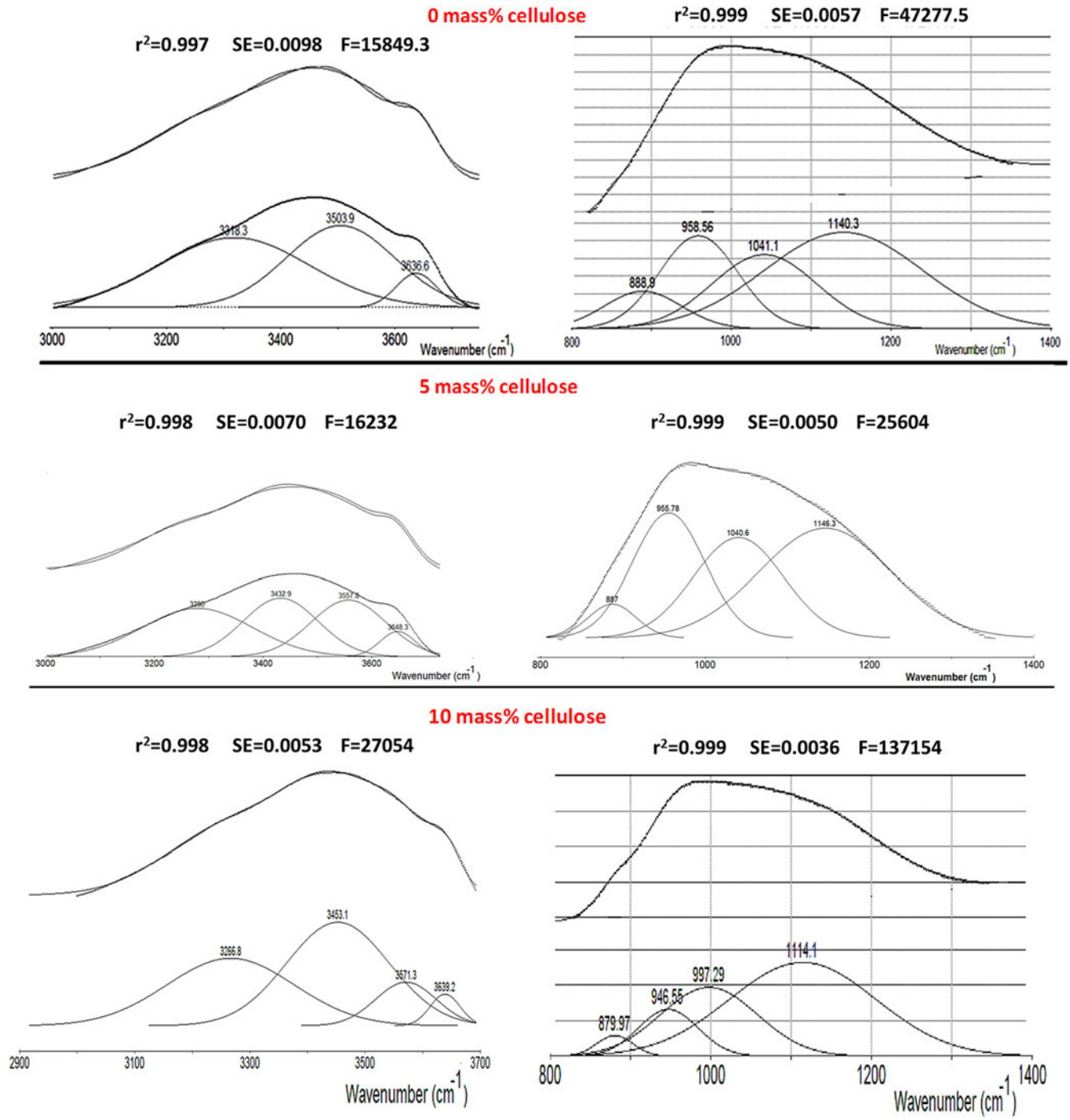

Figure 10. Deconvolution plots of the broad FTIR bands in the ranges of 3000–3700 and 800–1400 cm^{-1}.

Results and discussion

Microstructure characterization

Based on the XRD traces shown in Fig. 6, zeolite ZK-14 (PDF #84-0693) and sodium carbonate (PDF #86-0298) were formed in all cured alkali-activated samples. In line with the results of Valentini (2018), carbonation occurred in the alkali-activated metakaolin samples. According to Valentini (2018) and Zhang *et al.* (2014), such carbonation is the result of the presence of excess Na ions in the pore solution, and it occurred according to the following reactions:

$$CO_2(g) + 2OH^-(aq) \rightarrow CO_3^{2-}(aq) + H_2O$$

$$2Na^+(aq) + CO_3^{2-}(aq) + xH_2O \rightarrow Na_2CO_3 \cdot xH_2O\ (s)$$

Referring once again to Fig. 6, the formation of hydrosodalite (PDF#76-1639) was suspected seeing as its main X-ray reflections

https://doi.org/10.1180/clm.2024.6 Published online by Cambridge University Press

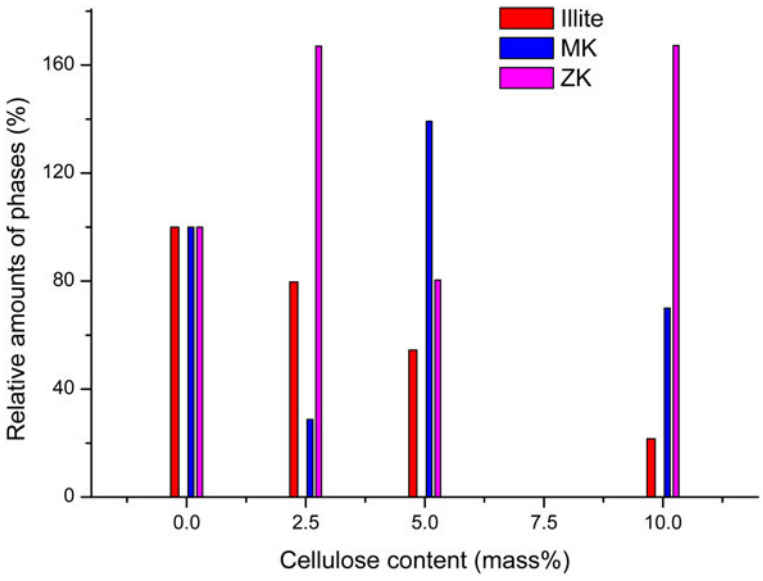

Figure 11. Variation of the relative amounts of zeolite ZK-14 (ZK), metakaolin (MK) and illite as a function of cellulose content.

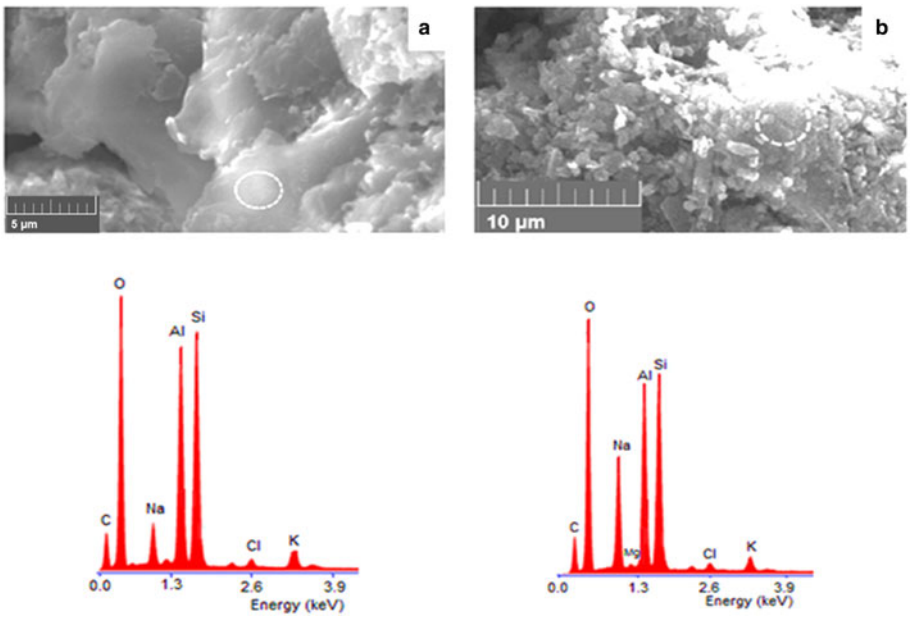

Figure 12. SEM images showing geopolymer-rich zones and their corresponding energy-dispersive spectroscopy spectra: (a) 0 mass% cellulose; (b) 10 mass% cellulose.

(°2θ = 14.09 (6.286 Å), 24.53 (3.629 Å)) are overlapped with those of zeolite ZK-14 (°2θ = 14.02 (6.314 Å), 24.41 (3.646 Å)). According to Król *et al.* (2017), the formation of sodalite can be explained thermodynamically due to the higher stability of its denser lattice.

As expected, scanning electron microscopy (SEM) examination (Figs 7 & 8) revealed pseudo-granular particles identified as hydrosodalite together with elongated particles associated with zeolite ZK-14 particles. A careful examination of the microstructure displayed hydrosodalite-free zones in the vicinity of zeolite ZK-14 particles. This could be related to the differences in the nucleation and the coalescence processes of these zeolites or to the elemental heterogeneity across the matrix. Discussion of zeolite formation is provided below.

FTIR spectroscopy analysis of the cured the samples indicated bands associated with metakaolin, illite, quartz and carbonate (Fig. 9). The zeolite/geopolymer bands could not be identified with certainty because of the bands overlapping. Therefore, the broad bands in the ranges of 3000–3700 and 800–1400 cm^{-1} were deconvoluted (Fig. 10). The bands at 3504–3571 and 958–946 cm^{-1} were associated with zeolites (Hajjaji, 2014; El Hafid & Hajjaji, 2015, 2018; Mourak *et al.*, 2021). Based on the areas of the FTIR spectroscopy bands of the zeolites, metakaolin and illite, the amounts of the two former minerals evolved antagonistically, whereas that of illite slightly declined as the cellulose content increased (Fig. 11). Due to the fact that metakaolin is a precursor of zeolite (Khaled *et al.*, 2023; Maruoka *et al.*, 2023), the increase in the zeolite content should be accompanied by decreased metakaolin contents and vice versa. The unexpected presence of metakaolin in the cured samples could be due to the limited access of OH^- ions to the embedded metakaolin

https://doi.org/10.1180/clm.2024.6 Published online by Cambridge University Press

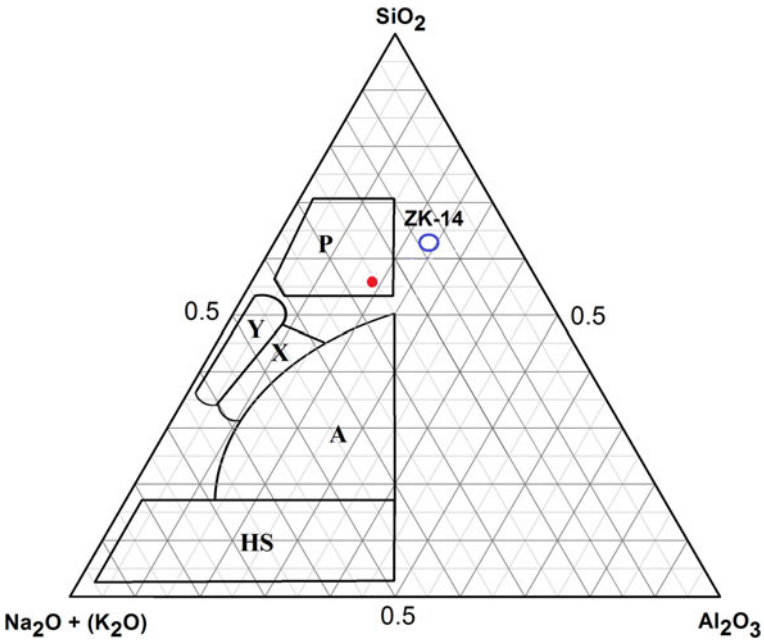

Figure 13. Ternary diagram showing the stability domains of zeolites (P, Y, X, A and HS; Xu *et al.*, 2009). The location of the zeolite ZK-14 (ZK-14) is introduced. The representative point of the cured sample is indicated in red.

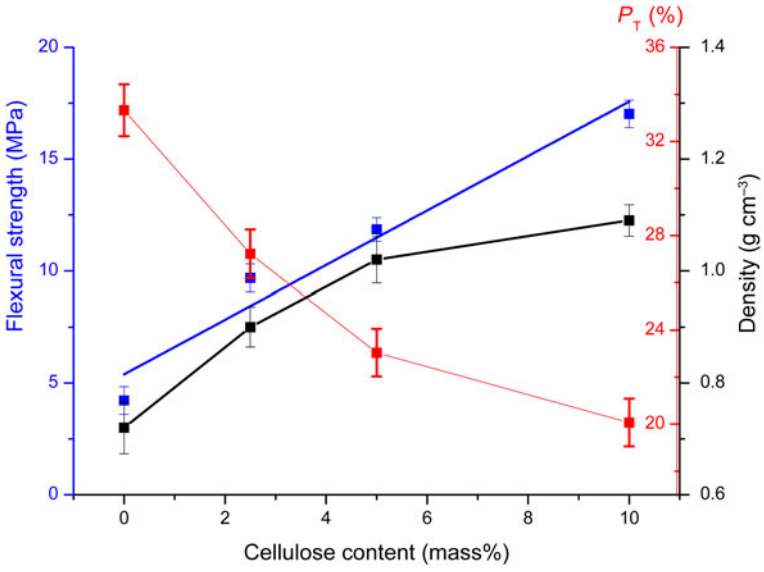

Figure 14. Variations in the mechanical and physical properties of the cured samples against cellulose content.

particles and to the interaction between OH^- ions and cellulose chains (mercerization reaction; Okano & Sarko, 1985; Nishimura *et al.*, 1991).

SEM examination showed that the microstructure of the cured samples was composed of zones such as those shown in Fig. 12. The features of such domains did not resemble those of the above-identified zones, and their Al/Si atomic ratios were almost constant (~1). By contrast, their (Na,K)/Si atomic ratios varied between 1.25 and 0.60. In this respect, it is worth noting that the atomic ratios of Si/Al, Si/Na and Al/Na of the used material were 1.4, 1.0 and 0.74, respectively. It was believed that the aforementioned domains corresponded to the areas of the geopolymer that was consisted of poly(sialate) units (Al/Si = 1; Zibouche *et al.*, 2009; Chen *et al.*, 2022). However, it should be noted that the geopolymer and hydrosodalite chemical compositions were quite similar. Therefore, it could be assumed that geopolymer was a precursor of hydrosodalite formation.

Regarding the ternary diagram (SiO_2–Al_2O_3–Na_2O) that delimits the stability domains of zeolites and the chemical composition of the cured cellulose-free sample, the elemental representative point of the sample fell within the zeolite P domain (Fig. 13). The mismatch between the detected zeolites (zeolite ZK-14 and hydrosodalite) and the expected one could be essentially due to sample heterogeneity and consequently to the difference in the spatial distribution of oxides. In fact, the formation of zeolite ZK-14 required a large amount of silica (~63 mass%) and relatively low contents of Al_2O_3 (~22.9 mass%) and Na_2O (~14.1 mass%). By contrast, hydrosodalite is supposed to occur in matrix locations where the contents of silica, alumina and sodium oxide are below 19, 39 and 42 mass%, respectively.

https://doi.org/10.1180/clm.2024.6 Published online by Cambridge University Press

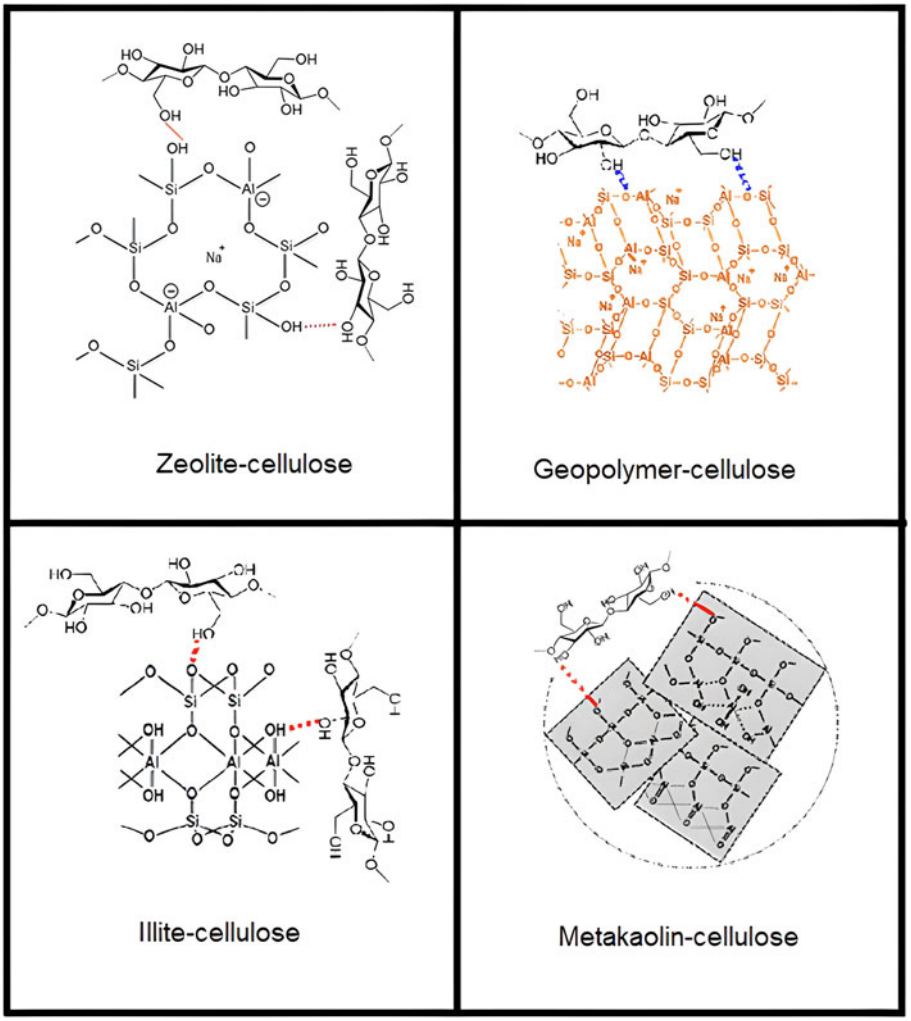

Figure 15. Schematic representations of hydrogen bonds that occurred between cellulose and the cured sample constituents (zeolite, geopolymer, illite and metakaolin).

Mechanical and physical properties

The flexural strength of the cured samples increased almost linearly with increasing cellulose content (Fig. 14). Amongst the mechanisms that might be involved in the strengthening process are the formation and the intensification of bonds between the cellulose fibres and sample constituents, the homogeneous distribution of the fibres and pores and porosity reduction (Ye *et al.*, 2018; Mourak *et al.*, 2021; Zheng *et al.*, 2023).

Regarding the influence of porosity on the mechanical strength of the cured samples, the results indicated that porosity decreased with increasing cellulose content (Fig. 14), and its evolution affected the flexural strength as follows:

$$\sigma_{FS}\ (\text{MPa}) = 5.39 - 5.47\ln\left(\frac{P_T\ -\ 18.3}{15}\right)\ (r^2_{adj} = 0.94)$$

The addition of cellulose also resulted in sample densification (Fig. 14). Therefore, the compaction process played a key role in sample strengthening. Moreover, the co-presence of zeolite and geopolymers induced an increase in the mechanical strength, as zeolite particles act as fillers (Andrejkovičová *et al.*, 2016). It was believed that the sample strengthening was essentially linked to the formation of hydrogen bonds between the functional moieties of cellulose and the active sites of the remaining sample constituents. To this point, it was observed that the FTIR spectroscopy band at 3504 cm^{-1}, which was associated with the stretching vibrations of the OH of zeolite attached to the Na^+ ions (Szostak, 1992), shifted as the addition of cellulose increased

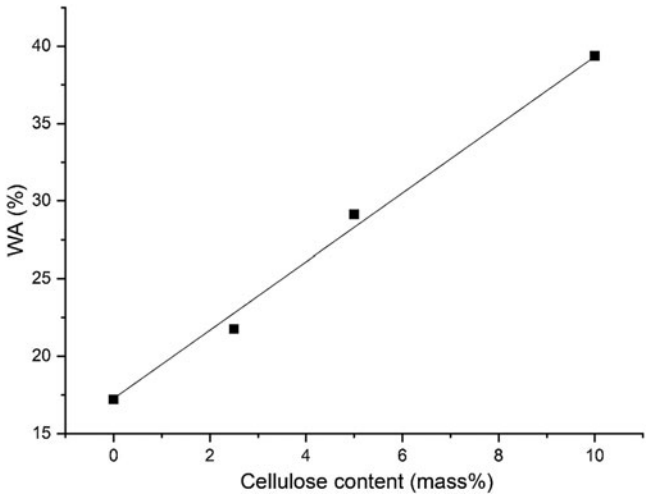

Figure 16. Evolution of water absorption (WA) by the cured samples as a function of cellulose content.

https://doi.org/10.1180/clm.2024.6 Published online by Cambridge University Press

Table 2. Flexural strengths of some fibre-reinforced geopolymer composites.

Fibre	Flexural strength (MPa)	Reference
Cotton	5.85	Korniejenko *et al.* (2016)
Sisal	5.90	
Jute	5.40	Silva *et al.* (2019)
Kenaf	6.08	Abbas *et al.* (2023)
Sawdust	10.20	Duan *et al.* (2016)
Oil palm trunk	4.12	Kavipriya *et al.* (2021)
Carbon	3.90–5.10	Nuaklong *et al.* (2021)
Cellulose	Up to 17	This study

(54 and 67 cm^{-1} for samples with 5 and 10 mass% cellulose, respectively; Fig. 10). Schematic representations of such a bond and the hydrogen bonds between the cellulose and the other constituents are provided in Fig. 15.

The increase in cellulose content led to increased water absorption, as shown in Fig. 16. This cannot be associated with sample porosity because it was shown that porosity continuously decreased with increasing cellulose content. In this context, it was believed that the measured amount of adsorbed water was an average value of the water amounts retained in the open and connected pores and by zeolites, geopolymers and cellulose fibres.

The products obtained could be used as lightweight mortars as well as binders for brick manufacturing. As compared with some natural fibre-reinforced geopolymer composites, the studied products had high flexural strength (Table 2).

Conclusion

The results of this study yielded the following conclusions:

(1) A Moroccan clay that consisted of kaolinite, pyrophyllite and illite (the main clay mineral) was thermally activated by heating at 700°C for 2 h for geopolymer synthesis. Due to the heating, kaolinite underwent dehydroxylation at ∼523°C, whereas illite and pyrophyllite resisted heating up to ∼900°C. The clay heating resulted in the formation of metakaolin, which is considered to be a high-grade aluminosilicate, for the geopolymer preparation. The heated clay was mixed with cellulose (up to 10 mass%), which was extracted from date palm (*P. dactylifera*) rachis, and alkali-activated with NaOH solution (6 M). The samples prepared were cured at 83°C for 30 days under an open atmosphere.

(2) As a result of curing, hydrosodalite, zeolite ZK-14, Na-carbonate and a geopolymer composed of poly(sialate) units (Al/Si atomic ratio = 1) were formed. The formation of these compounds, which was in line with some previous studies dealing with the geopolymerization of fly ash- or metakaolin-based source materials, was discussed in relation to the literature data.

(3) Metakaolin as well as illite were found in all of the studied samples. The relative amounts of metakaolin and zeolites evolved in opposite directions with the addition of cellulose, whereas that of illite slightly decreased. Zeolites were relatively abundant in the cured samples containing 2.5 and 10 mass% cellulose. However, it was believed that because of the low to moderate PD (892) of the cellulose, the fibres were well dispersed throughout the matrix because no bundles were observed at the SEM magnification (20 000×) used.

(4) Cellulose addition improved the performances of the cured samples as it increased their mechanical strength and reduced their porosity. In addition, it resulted in their densification. Taking, for instance, the sample containing 10 mass% cellulose, the strength/density ratio was enhanced by ∼17%. This performance improvement was mainly attributed to hydrogen bonds between the functional groups of cellulose and the active sites of the formed aluminosilicate minerals as well as metakaolin.

(5) As compared with some natural fibre-reinforced geopolymer composites, the studied cured mixtures had high mechanical strength. They could be used as lightweight mortars or as binders for brick manufacturing.

Conflicts of interest. The authors declare none.

References

Abbas A.G.N., Aziz F.N.A.A., Abdan K., Nasir N.A.M. & Huseien G.F. (2023) Experimental evaluation and statistical modeling of kenaf fiber-reinforced geopolymer concrete. *Construction and Building Materials*, **367**, 130228.

Almutairi A.L., Tayeh B.A., Adesina A., Isleem H.F. & Zeyad A.M. (2021) Potential applications of geopolymer concrete in construction: a review. *Case Studies in Construction Materials*, **15**, e00733.

Andrejkovičová S., Sudagar A., Rocha J., Patinha C., Hajjaji W., da Silva E.F. *et al.* (2016) The effect of natural zeolite on microstructure, mechanical and heavy metals adsorption properties of metakaolin based geopolymers. *Applied Clay Science*, **126**, 141–152.

Aravindh M., Sathish S., Ranga Raj R., Karthick A., Mohanavel V., Patil P.P. *et al.* (2022) A review on the effect of various chemical treatments on the mechanical properties of renewable fiber-reinforced composites. *Advances in Materials Science and Engineering*, **2022**, 2009691.

Asyraf M.R.M., Syamsir A., Supian A.B.M., Usman F., Ilyas R.A., Nurazzi N.M. *et al.* (2022) Sugar palm fibre-reinforced polymer composites: influence of chemical treatments on its mechanical properties. *Materials*, **15**, 3852.

Ayub F. & Khan S.A. (2023) An overview of geopolymer composites for stabilization of soft soils. *Construction and Building Materials*, **404**, 133195.

Bashline L., Lei L., Li S. & Gu Y. (2014) Cell wall, cytoskeleton, and cell expansion in higher plants. *Molecular Plant*, **7**, 586–600.

Chen S., Wang K., Wei E., Muhammad Y., Yi M., Wei Y. & Fujita T. (2022) Preparation of Al_2O_3-$2SiO_2$/geopolymer powder by hydrolytic sol-gel method and its activity characterization and research on the reaction mechanism. *Powder Technology*, **397**, 117026.

Chen X., Wang K., Wang Z., Zeng H., Yang T. & Zhang X. (2021) Highly stretchable composites based on cellulose. *International Journal of Biological Macromolecules*, **170**, 71–87.

da Silva Rego J.H., Sanjuán M.Á., Mora P., Zaragoza A. & Visedo G. (2023) Carbon dioxide uptake by Brazilian cement-based materials. *Applied Sciences*, **13**, 10386.

de Souza L.O., Liebscher M., de Souza L.M.S., de Andrade Silva F. &, Mechtcherine V. (2023) Effect of microcrystalline and nano-fibrillated cellulose on the mechanical behavior and microstructure of cement pastes. *Construction and Building Materials*, **408**, 133812.

dos Reis R.R., Effting C. & Schackow A. (2023) Cellulose nanofibrils on lightweight mortars for improvement of the performance of cement systems. *Carbohydrate Polymer Technologies and Applications*, **5**, 100303.

Duan P., Yan C., Zhou W. & Luo W. (2016) Fresh properties, mechanical strength and microstructure of fly ash geopolymer paste reinforced with sawdust. *Construction and Building Materials*, **111**, 600–610.

El Hafid K. & Hajjaji M. (2015) Effects of the experimental factors on the microstructure and the properties of cured alkali-activated heated clay. *Applied Clay Science*, **116**, 202–210.

El Hafid K. & Hajjaji M. (2018) Geopolymerization of glass- and silicate-containing heated clay. *Construction and Building Materials*, **159**, 598–609.

Emenike E.C., Iwuozor K.O., Saliu O.D., Ramontja J. & Adeniyi A.G. (2023) Advances in the extraction, classification, modification, emerging and

advanced applications of crystalline cellulose: a review. *Carbohydrate Polymer Technologies and Applications*, **6**, 100337.
Etale A., Onyianta A.J., Turner S.R. & Eichhorn S.J. (2023) Cellulose: a review of water interactions, applications in composites, and water treatment. *Chemical Reviews*, **123**, 2016–2048.
Evans R. & Wallis A.F. (1989) Cellulose molecular weights determined by viscometry. *Journal of Applied Polymer Science*, **37**, 2331–2340.
Farhan K.Z., Johari M.A.M. & Demirboğa R. (2021) Impact of fiber reinforcements on properties of geopolymer composites: a review. *Journal of Building Engineering*, **44**, 102628.
Ferreira S.R., Ukrainczyk N., e Silva K.D.D.C., Silva L.E. & Koenders E. (2021) Effect of microcrystalline cellulose on geopolymer and Portland cement pastes mechanical performance. *Construction and Building Materials*, **288**, 123053.
Giacobello F., Ielo I., Belhamdi H. & Plutino M.R. (2022) Geopolymers and functionalization strategies for the development of sustainable materials in construction industry and cultural heritage applications: a review. *Materials*, **15**, 1725.
Gualtieri A.F. & Ferrari S. (2006) Kinetics of illite dehydroxylation. *Physics and Chemistry of Minerals*, **33**, 490–501.
Hajjaji M. (2014) Minéralogie et transformation thermique des matériaux argileux de la région de Marrakech, Maroc. *Comunicaçõe Geológicas*, **101**, 75–80.
Hallac B.B. & Ragauskas A.J. (2011) Analyzing cellulose degree of polymerization and its relevancy to cellulosic ethanol. *Biofuels, Bioproducts and Biorefining*, **5**, 215–225.
Heah C.Y., Kamarudin H., Al Bakri A.M., Binhussain M., Luqman M., Nizar I.K. *et al.* (2011) Effect of curing profile on kaolin-based geopolymers. *Physics Procedia*, **22**, 305–311.
Jaberizadeh M.M., Danoglidis P.A., Shah S.P. & Konsta-Gdoutos M.S. (2023) Eco-efficient cementitious composites using waste cellulose fibers: effects on autogenous shrinkage, strength and energy absorption capacity. *Construction and Building Materials*, **408**, 133504.
Jamshaid H., Mishra R.K., Raza A., Hussain U., Rahman M.L., Nazari S. *et al.* (2022) Natural cellulosic fiber reinforced concrete: influence of fiber type and loading percentage on mechanical and water absorption performance. *Materials*, **15**, 874.
Jwaida Z., Dulaimi A., Mashaan N. & Othuman Mydin M.A. (2023) Geopolymers: the green alternative to traditional materials for engineering applications. *Infrastructures*, **8**, 98.
Kavipriya S., Deepanraj C.G., Dinesh S., Prakhash N., Lingeshwaran N. & Ramkumar S. (2021) Flexural strength of lightweight geopolymer concrete using sisal fibres. *Materials Today: Proceedings*, **47**, 5503–5507.
Khaled Z., Mohsen A., Soltan A. & Kohail M. (2023) Optimization of kaolin into metakaolin: calcination conditions, mix design and curing temperature to develop alkali activated binder. *Ain Shams Engineering Journal*, **14**, 102142.
Korniejenko K., Frączek E., Pytlak E. & Adamski M. (2016) Mechanical properties of geopolymer composites reinforced with natural fibers. *Procedia Engineering*, **151**, 388–393.
Król M., Rożek P. & Mozgawa W. (2017) Synthesis of the sodalite by geopolymerization process using coal fly ash. *Polish Journal of Environmental Studies*, **26**, 2611–2617.
Lazorenko G., Kasprzhitskii A., Mischinenko V. & Kruglikov A. (2022) Fabrication and characterization of metakaolin-based geopolymer composites reinforced with cellulose nanofibrils. *Materials Letters*, **308**, 131146.
Malešič J., Kraševec I. & Kralj Cigić I. (2021) Determination of cellulose degree of polymerization in historical papers with high lignin content. *Polymers*, **13**, 1990.
Maruoka L.M., Pinheiro I.F., Freitas H.S., Nobre F.X. & Scalvi L.V. (2023) Effect of thermal annealing on kaolin from the Amazon region, aiming at the production of geopolymer. *Journal of Materials Research and* Technology, **25**, 2471–2485.
Mijarsh M.J.A., Johari M.M. & Ahmad Z.A. (2015) Effect of delay time and Na_2SiO_3 concentrations on compressive strength development of geopolymer mortar synthesized from TPOFA. *Construction and Building Materials*, **86**, 64–74.
Mo B.H., Zhu H., Cui X.M., He Y. & Gong S.Y. (2014) Effect of curing temperature on geopolymerization of metakaolin-based geopolymers. *Applied Clay Science*, **99**, 144–148.
Mohamad N., Muthusamy K., Embong R., Kusbiantoro A. & Hashim M.H. (2022) Environmental impact of cement production and solutions: a review. *Materials Today: Proceedings*, **48**, 741–746.
Mourak A., Hajjaji M. & Alagui A. (2021) Cured alkali-activated heated clay–cellulose composites: microstructure, effect of glass addition and performances. *Boletín de la Sociedad Española de Cerámica y Vidrio*, **60**, 62–72.
Nishimura H., Okano T. & Sarko A. (1991) Mercerization of cellulose. 5. Crystal and molecular structure of Na-cellulose I. *Macromolecules*, **24**, 759–770.
Nuaklong P., Wongsa A., Boonserm K., Ngohpok C., Jongvivatsakul P., Sata V. *et al.* (2021) Enhancement of mechanical properties of fly ash geopolymer containing fine recycled concrete aggregate with micro carbon fiber. *Journal of Building Engineering*, **41**, 102403.
Okano T. & Sarko A. (1985) Mercerization of cellulose. II. Alkali–cellulose intermediates and a possible mercerization mechanism. *Journal of Applied Polymer Science*, **30**, 325–332.
Raghunath S., Hoque M. & Foster E.J. (2023) On the roles of cellulose nanocrystals in fiber cement: implications for rheology, hydration kinetics, and mechanical properties. *ACS Sustainable Chemistry & Engineering*, **11**, 10727–10736.
Ranjbar N., Kuenzel C., Spangenberg J. & Mehrali M. (2020) Hardening evolution of geopolymers from setting to equilibrium: a review. *Cement and Concrete Composites*, **114**, 103729.
Santana H.A., Júnior N.S.A., Ribeiro D.V., Cilla M.S. & Dias C.M. (2021) Vegetable fibers behavior in geopolymers and alkali-activated cement based matrices: a review. *Journal of Building Engineering*, **44**, 103291.
Segal L.G., Creely J.J., Martin Jr A.E. & Conrad C.M. (1957) An empirical method for estimating the degree of crystallinity of native cellulose using the X-ray diffractometer. *Textile Research Journal*, **29**, 786–794.
Semugaza G., Mielke T., Castillo M.E., Gierth A.Z., Tam J.X., Nawrath S. & Lupascu D.C. (2023) Reactivation of hydrated cement powder by thermal treatment for partial replacement of ordinary Portland cement. *Materials and Structures,* **56**, 48.
Shi W., Sha Z., Qiao F., Tang W., Luo C., Zheng Y. *et al.* (2023) Study on the temporal and spatial evolution of China's carbon dioxide emissions and its emission reduction path. *Energies*, **16**, 829.
Silva G., Salirrosas J., Ruiz G., Kim S., Nakamatsu J. & Aguilar R. (2019) Evaluation of fire, high-temperature and water erosion resistance of fiber-reinforced lightweight pozzolana-based geopolymer mortars. *IOP Conference Series: Materials Science and Engineering*, **706**, 012016.
Singh H. & Gupta R. (2020) Influence of cellulose fiber addition on self-healing and water permeability of concrete. *Case Studies in Construction Materials*, **12**, e00324.
Sotelo-Piña C., Aguilera-González E.N. & Martínez-Luévanos A. (2019) Geopolymers: past, present, and future of low carbon footprint eco-materials. *Handbook of Ecomaterials*, **4**, 2765–2785.
Szostak R. (1992). *Handbook of Molecular Sieves*. Van Nostrand Reinhold, New York, NY, USA, 557 pp.
Tanu H.M. & Unnikrishnan S. (2022) Utilization of industrial and agricultural waste materials for the development of geopolymer concrete – a review. *Materials Today: Proceedings*, **65**, 1290–1297.
Valentini L. (2018) Modeling dissolution–precipitation kinetics of alkali-activated metakaolin. *ACS Omega*, **3**, 18100–18108.
Van Deventer J.S.J., Provis J.L., Duxson P. & Lukey G.C. (2007) Reaction mechanisms in the geopolymeric conversion of inorganic waste to useful products. *Journal of Hazardous Materials*, **139**, 506–513.
Van Jaarsveld J.G.S., Van Deventer J.S. & Lukey G.C. (2002) The effect of composition and temperature on the properties of fly ash- and kaolinite-based geopolymers. *Chemical Engineering Journal*, **89**, 63–73.
Weng L. & Sagoe-Crentsil K. (2007) Dissolution processes, hydrolysis and condensation reactions during geopolymer synthesis: part I – low Si/Al ratio systems. *Journal of Materials Science*, **42**, 2997–3006.
Ye H., Zhang Y., Yu Z. & Mu J. (2018) Effects of cellulose, hemicellulose, and lignin on the morphology and mechanical properties of metakaolin-based geopolymer. *Construction and Building Materials*, **173**, 10–16.

https://doi.org/10.1180/clm.2024.6 Published online by Cambridge University Press

Zhang J., Yang H., Zhang S., Feng T. & Li Y. (2023) Potential utilization of CO_2 foams in developing lightweight building materials. *Journal of Building Engineering*, **76**, 107342.

Zhang Z., Provis J.L., Reid A. & Wang H. (2014) Fly ash-based geopolymers: the relationship between composition, pore structure and efflorescence. *Cement and Concrete Research*, **64**, 30–41.

Zheng Y., Wang Z., Wan Z., Yang X., Lin F., Chen Y. *et al.* (2023) Mechanochemical fabrication of geopolymer composites based on the reinforcement effect of microfibrillated cellulose. *Ceramics International*, **49**, 503–511.

Zibouche F., Kerdjoudj H., de Lacaillerie J.B.D.E. & Van Damme H. (2009) Geopolymers from Algerian metakaolin. influence of secondary minerals. *Applied Clay Science*, **43**, 453–458.

https://doi.org/10.1180/clm.2024.6 Published online by Cambridge University Press